Floating Random Walk-Based Capacitance Simulation Considering General Floating Metals

Wenjian Yu, *Senior Member, IEEE*, Zhezhao Xu, Bo Li, and Cheng Zhuo, *Senior Member, IEEE*

***Abstract*—Accurate capacitance calculation for structures including floating metals is of great interest to both the modeling of interconnect wires and the verification of on-chip capacitors in the design of integrated circuit. The former problem involves regular-shape or cuboid floating dummy fills, and has been addressed with an existing fast algorithm based on floating random walk (FRW) method. The latter problem involves floating metals in more general and complex shape, and is crucial for the design of high-density metal–insulator–metal (MIM) capacitor which endures higher voltage. How to efficiently handle these general-shape floating metals becomes a challenge. In this paper, we first investigate the mechanism of the existing FRW-based approach for handling floating dummies, and then propose an approach based on the central difference formula for handling the general-shape floating metals. The proposed approach has comparable cost to the existing work, but is much more reliable and accurate. Experiments on the structures with floating dummies and MIM capacitor structures have validated the effectiveness and advantage of the proposed approach.**

***Index Terms*—Capacitance calculation, floating metal, floating random walk (FRW) method, metal–insulator–metal (MIM) capacitor.**

I. Introduction

Capacitance extraction for interconnect parasitics modeling is the basis of accurate circuit simulation and physical verification for quality IC design. Similar problem arises in the design of on-chip metal-insulator-metal (MIM) capacitor. High-density MIM capacitor has been widely adopted as an efficient alternative to on-die decoupling [1], [5]. As shown in Fig. 1(a), the conventional MIM structure embedded in two top metal layers is featured with a thin dielectric. Due to the concern of dielectric breakdown in high voltage domains, floating metal plate was recently introduced to the MIM capacitor [2], [3]. Fig. 1(b) and (c) demonstrate two examples of the MIM capacitor with floating metals. This produces floating metals with irregular geometry due to the constraints of via patterns and interconnect routing, and further complicates the calculation of MIM structure's capacitance. Therefore, an efficient yet accurate method for such capacitance calculation is highly desired.

The floating metals, also known as the dummies inserted around interconnect wires for design-for-manufacture concern, are not normal conductor in capacitance extraction. The electric charge on each floating metal equals to zero. Their presence affects the capacitances of surrounding normal conductors. A straightforward treatment is regarding floating metals as normal electrodes and extracting full capacitance matrix, and then reducing the matrix to obtain the equivalent capacitances among normal conductors. This is called network reduction method [4]. More efficient techniques have been proposed based on boundary element method [6] or floating random walk (FRW) method [4], which avoids the generation and reduction of the full capacitance matrix. It should be pointed out that the approach in [4] assumes either a simple transition scheme jumping from floating metal or that the corresponding transition probabilities are precomputed and stored. Thus, it is not suitable for handling floating metals with arbitrarily geometry, and may induce significant error.

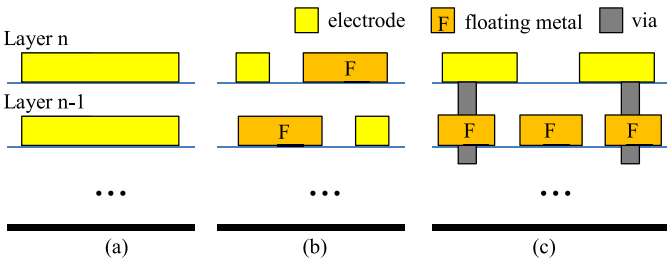

Fig. 1. Cross section view of the integrated capacitors. (a) Conventional MIM capacitor. (b) and (c) Two MIM capacitors with floating metals.

In this paper, we consider general-shape floating metals, such as the multirectangle shape seen in the design of MIM capacitors, and develop a reliable and efficient FRW-based technique for the capacitance calculation problem. We first relate the approach in [4] to the electric neutrality equation, and reveal its theoretic flaw due to the simple transition scheme. Then, based on the central difference formula to approximate partial derivative we propose a new approach that involves a special integral surface enclosing each floating metal and the corresponding transition scheme. The approach does not require the offline computation for each kind of floating metal, and induces much less systematic error. Finally, we extend the approach to handle multirectangle floating metal and the structure in multidielectric environment. Numerical experiments on the structures with floating dummies and MIM capacitor have validated the accuracy of the proposed approach. Compared with the approach in [4], it has much better stableness, with up to 5× reduction on the systematic error. If keeping the systematic errors of both methods within 0.5% (as compared to Raphael's result), the proposed approach can be over 3.7× faster than the extension of the approach in [4].

II. Background

A. FRW Algorithm for 3-D Capacitance Extraction

The FRW method for calculating electrostatic capacitance is originated from expressing the electric potential of a point $\boldsymbol{r}$ as an integral of the potential on surface S enclosing $\boldsymbol{r}$ [7], [8]

$$\phi(\boldsymbol{r}) = \oint_S P(\boldsymbol{r}, \boldsymbol{r}^{(1)})\phi(\boldsymbol{r}^{(1)})\mathrm{d}\boldsymbol{r}^{(1)}, \quad (1)$$

Manuscript received July 2, 2017; revised October 3, 2017 and November 29, 2017; accepted December 8, 2017. Date of publication December 13, 2017; date of current version July 17, 2018. This work was supported by NSFC under Grant 61422402 and Grant 61601406. This paper was recommended by Associate Editor A. Srivastava. *(Corresponding authors: Wenjian Yu; Cheng Zhuo.)*

W. Yu, Z. Xu, and B. Li are with the TNList, Department of Computer Science and Technology, Tsinghua University, Beijing 100084, China (e-mail: yu-wj@tsinghua.edu.cn).

C. Zhuo is with the College of Information Science and Electronics Engineering, Zhejiang University, Hangzhou 310027, China (e-mail: czhuo@zju.edu.cn).

Color versions of one or more of the figures in this paper are available online at http://ieeexplore.ieee.org.

Digital Object Identifier 10.1109/TCAD.2017.2782770

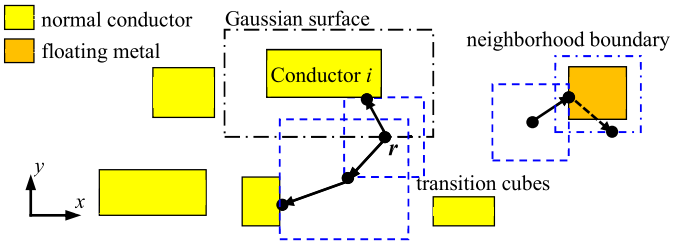

Fig. 2. Two random walks starting from $\boldsymbol{r}$ (denoted by arrows) in the FRW method, and a random walk encountering a floating metal (2-D top view).

where $P(\boldsymbol{r}, \boldsymbol{r}^{(1)})$ is called surface Green's function and can be regarded as a probability density function and $\mathrm{d}\boldsymbol{r}^{(1)}$ denotes infinitesimal area at position $\boldsymbol{r}^{(1)}$. Therefore, $\phi(\boldsymbol{r})$ is the statistical mean of $\phi(\boldsymbol{r}^{(1)})$, and can be calculated with a Monte Carlo procedure sampling S. The domain enclosed by S is called transition domain, and usually $\boldsymbol{r}$ is at its center.

In the problem of capacitance calculation, usually the coupling capacitances between a conductor i and other conductors are wanted. With the FRW method, a Gaussian surface G_i is constructed to enclose conductor i (see Fig. 2). According to the Gauss theorem, the charge of conductor i

$$Q_i = \oint_{G_i} \varepsilon(\boldsymbol{r}) g \int_{S^{(1)}} \omega(\boldsymbol{r}, \boldsymbol{r}^{(1)}) q(\boldsymbol{r}, \boldsymbol{r}^{(1)}) \phi(\boldsymbol{r}^{(1)}) \mathrm{d}\boldsymbol{r}^{(1)} \mathrm{d}\boldsymbol{r}, \tag{2}$$

where $\varepsilon(\boldsymbol{r})$ is the dielectric permittivity at point $\boldsymbol{r}$, $q(\boldsymbol{r}, \boldsymbol{r}^{(1)})$ is the probability density function for sampling on $S^{(1)}$, the surface of a transition domain. g is a constant, which satisfies $\oint_{G_i} \varepsilon(\boldsymbol{r}) g \mathrm{d}\boldsymbol{r} = 1$. $q(\boldsymbol{r}, \boldsymbol{r}^{(1)})$ may be different from $P(\boldsymbol{r}, \boldsymbol{r}^{(1)})$, and $\omega(\boldsymbol{r}, \boldsymbol{r}^{(1)})$ is the weight value [7]. Thus, Q_i can be estimated as the statistical mean of sampled values on G_i, which is further the mean of sampled potentials on $S^{(1)}$ multiplying the weight value. If the sampled potential is unknown, this spatial sampling procedure will repeat until a point with known potential is obtained (e.g., on conductor surface). It forms an FRW including a sequence of hops. Each hop is from the center of a transition domain to its boundary. With a number of such walks, the statistical mean of the weight values for the walks terminating at conductor j approximates the coupling capacitance C_{ij} (if $j \neq i$), or the self-capacitance C_{ii}.

B. FRW Technique Considering Floating Dummy-Fills

For the structure with floating dummies, the FRW method was modified in [4] to directly calculate the equivalent capacitances among normal conductors. Not like the network reduction method, it does not treat floating metal as normal conductor. Therefore, the random walk does not terminate at a floating metal, and instead continues with the next position randomly selected on a neighborhood boundary. This is shown in Fig. 2, and the neighborhood boundary is a closed *sampling surface*. The modified FRW algorithm is described as follows.

The random transition from a floating metal F is explained with the formula of its electric potential [4]

$$\phi(F) = \oint_{\Gamma_f} \frac{\tilde{\varepsilon}(\boldsymbol{r})}{K \cdot t(\boldsymbol{r})} \phi(\boldsymbol{r}) \mathrm{d}\boldsymbol{r}, \quad K = \oint_{\Gamma_f} \frac{\tilde{\varepsilon}(\boldsymbol{r})}{t(\boldsymbol{r})} \mathrm{d}\boldsymbol{r}, \tag{3}$$

where Γ_f is the neighborhood boundary, $\tilde{\varepsilon}(\boldsymbol{r})$ is the average permittivity, and $t(\boldsymbol{r})$ is the average normal distance from each face of Γ_f to F. Notice that K is a constant, and $\tilde{\varepsilon}(\boldsymbol{r})/(K \cdot t(\boldsymbol{r}))$ in (3) can be thought of as a probability density function. Usually, the neighborhood boundary is set as the uniform inflation of the cuboid dummy fill. Otherwise, the transition probabilities have to be precomputed and stored for each floating metal [4].

Algorithm 1 Modified FRW Algorithm Handling Floating Dummy-Fills

1. Load the pre-calculated transition probabilities and weight values for the unit-size cubic domain;
2. For each floating metal-fill k, construct its neighborhood boundary Γ_k and calculate quantities for performing random sampling on Γ_k;
3. Construct the Gaussian surface enclosing conductor i;
4. $\boldsymbol{C}_{ij} \coloneqq 0, \forall j$; $npath \coloneqq 0$;
5. **Repeat**
6. $\quad npath \coloneqq npath + 1$;
7. $\quad$ Randomly pick a point $\boldsymbol{r}$ on the Gaussian surface, and generate a cubic transition domain S centered at $\boldsymbol{r}$; pick a point $\boldsymbol{r}^{(1)}$ on surface of S with the transition probabilities;
8. $\quad \omega \coloneqq \omega(\mathbf{r}, \mathbf{r}^{(1)})$ in (2);
9. $\quad$ **While** current point $\boldsymbol{r}^{(x)}$ is not on a normal conductor
10. $\quad\quad$ **If** $\mathbf{r}^{(x)}$ is on a floating metal k,
11. $\quad\quad\quad$ Randomly pick a point $\boldsymbol{r}^{(y)}$ on Γ_k;
12. $\quad\quad$ **Else**
13. $\quad\quad\quad$ Construct the transition cube taking floating metals as obstacles, and make a FRW hop to $\boldsymbol{r}^{(y)}$;
14. $\quad\quad$ **End**
15. $\quad\quad \boldsymbol{r}^{(x)} \coloneqq \boldsymbol{r}^{(y)}$;
16. $\quad$ **End**
17. $\quad C_{ij} \coloneqq C_{ij} + \omega$; // the current point is on conductor j
18. **Until** the convergence criterion is met
19. $C_{ij} \coloneqq C_{ij}/npath, \quad \forall j$.

Although the technique in [4] demonstrated high accuracy for structures including floating dummy fills, its theory is vague. More seriously, the simple neighborhood setting could induce large systematic error for general-shape floating metals, and the offline computation for each floating metal may not be feasible. More accurate technique for handling general floating metals, like in MIM capacitors, should be developed.

III. Approach Considering General-Shape Floating Metals

In this section, we first derive an approach based on the central difference formula for handling cuboid-shape floating metals. Then, we extend it to deal with multirectangle floating metals. Finally, we give more technical details.

A. Approach Based on the Central Difference Formula

We first look at (3), which implies:

$$\oint_{\Gamma_f} \frac{\tilde{\varepsilon}(\boldsymbol{r})}{t(\boldsymbol{r})} \phi(F) \mathrm{d}\boldsymbol{r} = \oint_{\Gamma_f} \frac{\tilde{\varepsilon}(\mathrm{r})}{t(\mathrm{r})} \phi(\mathrm{r}) \mathrm{d}\boldsymbol{r}, \text{ or} \tag{4}$$

$$\oint_{\Gamma_f} \tilde{\varepsilon}(\boldsymbol{r}) \frac{\phi(F) - \phi(\boldsymbol{r})}{t(\boldsymbol{r})} \mathrm{d}\boldsymbol{r} = 0. \tag{5}$$

This makes us to think of the electric neutrality equation for floating metal (applying the Gauss theorem)

$$Q(F) = \oint_{\Gamma_f} \varepsilon(\boldsymbol{r}) \frac{\partial \phi(\boldsymbol{r})}{\partial n(\boldsymbol{r})} \mathrm{d}\boldsymbol{r} = 0, \tag{6}$$

where $\partial\phi(\boldsymbol{r})/\partial n(\boldsymbol{r})$ denotes the outer normal electric field intensity at point $\boldsymbol{r}$. We realize that $(\phi(F) - \phi(\boldsymbol{r}))/t(\boldsymbol{r})$ in (5) can be regarded as the forward-difference approximation of the normal electric field intensity in (6) in some situation. However, when $\boldsymbol{r}$ is near a corner of the cuboid neighborhood boundary [see Fig. 3(a)], this does not hold. Notice that such explanation of (5) stands only if the floating metal is spherical [see Fig. 3(b)]. For general-shape floating metal, there is a lack of rationality in (5) or the approach of [4].

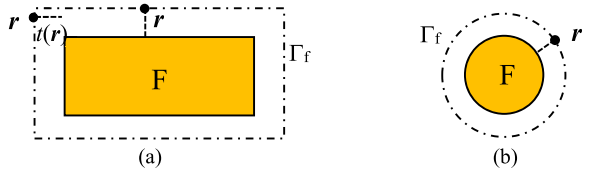

Fig. 3. (a) Illustration of the forward-difference approximation for cuboid-shape floating metal and (b) sphere-shape floating metal.

We now consider how to derive a more accurate approach for the cuboid-shape floating metal F with dimensions $l_1 \times l_2 \times l_3$. For any *integral surface* Γ enclosing F, we have

$$Q(F) = \oint_{\Gamma} \varepsilon(\boldsymbol{r}) \frac{\partial \phi(\boldsymbol{r})}{\partial n(\boldsymbol{r})} \mathrm{d}\boldsymbol{r} = 0. \tag{7}$$

Approximating the partial derivative in (7) with the central difference formula, we obtain

$$0 \approx \oint_{\Gamma} \varepsilon(\boldsymbol{r}) \frac{\phi(\boldsymbol{r}_{\text{out}}) - \phi(\boldsymbol{r}_{\text{in}})}{2s(\boldsymbol{r})} \mathrm{d}\boldsymbol{r}, \tag{8}$$

where $\boldsymbol{r}_{\text{in}}$ and $\boldsymbol{r}_{\text{out}}$ are two points such that the line connecting them intersects Γ perpendicularly at $\boldsymbol{r}$. And, $\boldsymbol{r}_{\text{in}}$ and $\boldsymbol{r}_{\text{out}}$ have the same distance $s(\boldsymbol{r})$ to point $\boldsymbol{r}$ (see Fig. 4). Assuming $\boldsymbol{r}_{\text{in}}$ is on F such that $\phi(\boldsymbol{r}_{\text{in}})$ equals to $\phi(F)$, we have

$$\left(\oint_{\Gamma} \frac{\varepsilon(\boldsymbol{r})}{s(\boldsymbol{r})} \mathrm{d}\boldsymbol{r}\right) \phi(F) \approx \oint_{\Gamma} \frac{\varepsilon(\boldsymbol{r})}{s(\boldsymbol{r})} \phi(\boldsymbol{r}_{\text{out}}) \mathrm{d}\boldsymbol{r}, \quad \text{or} \tag{9}$$

$$\phi(F) \approx \oint_{\Gamma} P_F(\boldsymbol{r}) \phi(\boldsymbol{r}_{\text{out}}) \mathrm{d}\boldsymbol{r} = \oint_{\Gamma} \frac{\varepsilon(\boldsymbol{r})}{K \cdot s(\boldsymbol{r})} \phi(\boldsymbol{r}_{\text{out}}) \mathrm{d}\boldsymbol{r}, \tag{10}$$

$$\text{where} \quad K = \oint_{\Gamma} \frac{\varepsilon(\boldsymbol{r})}{s(\boldsymbol{r})} \mathrm{d}\boldsymbol{r}. \tag{11}$$

Obviously, $P_F(\boldsymbol{r})$ is a probability density function, and (10) implies a random transition scheme from the floating metal F. Although (10) looks very similar to (3), the integrands in them are different. Instead of integrating the electric potential on the closed surface Γ_f, the integral in (10) involves the electric potential on possible locations of $\boldsymbol{r}_{\text{out}}$ which constitute an unclosed *sampling surface*.

To ensure the existence of $\boldsymbol{r}_{\text{in}}$ on F, we construct the integral surface Γ as that shown in Fig. 4. We first translate each face of F outward a distance and then connect these translated faces with bevel faces. These distances are denoted by s_1, s_2, s_3, s_4, s_5, and s_6, as shown in Fig. 4. The resulted Γ includes 26 faces: six faces obtained by translating the faces of F (denoted by type I), 12 faces each connecting two adjacent type-I faces (denoted by type II), and eight faces each connecting three type-II faces (denoted by type III). Fig. 5 depicts examples of the three kinds of faces, corresponding to those labeled by "I," "II," and "III" in Fig. 4(b). So far, we have derived a new approach for handling cuboid-shape floating metal. It has three differences to the approach in [4]: 1) $s(\boldsymbol{r})$ in (10) and $t(\boldsymbol{r})$ in (3) have different meaning; 2) in the approach of [4] the integral surface and sampling surface are a same closed surface (i.e., neighborhood boundary), while in our approach the former is a closed surface with 26 faces and the latter is unclosed; and 3) our approach is derived from (7) rigorously with the second-order central differentiation formula. Thus, it has less systematic error than the approach of [4] corresponding to the forward difference.

The remaining problem is how to perform random sampling according to (10). This is realized by first randomly picking a face of Γ according to integrals of $P_F(\boldsymbol{r})$ and then sampling a point on the selected face. The integrals on the three types of faces, denoted by I_1, I_2, and I_3, are calculated separately. Here, we ignore the effect of dielectric permittivity $\varepsilon(\boldsymbol{r})$ in $P_F(\boldsymbol{r})$. The constant K can also be ignored. Take the faces shown in Fig. 5 as examples. For type-I face, $P_F(\boldsymbol{r}) = 1/s_i$ $(i = 1, 2, \ldots, 6)$, and the corresponding integral is

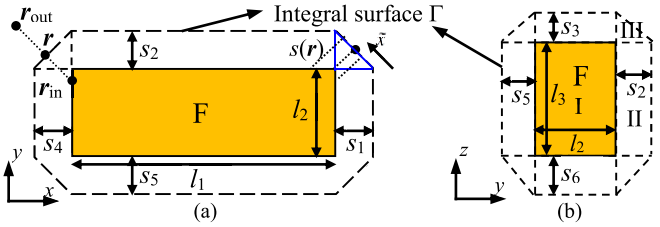

Fig. 4. Central difference formula-based approach with a special integral surface. (a) top view and (b) side view.

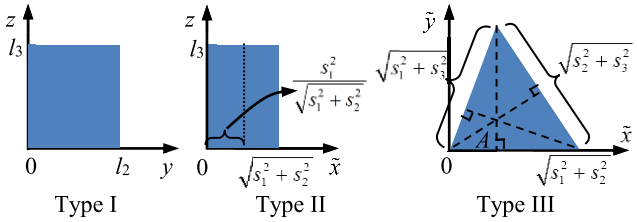

Fig. 5. Three types of faces of the integral surface (in local coordinates).

trivial. For type-II face, it corresponds to the hypotenuse of the blue triangle in Fig. 4(a). Along the $\tilde{x}$ direction $s(\boldsymbol{r})$ first decreases and then increases. The turning point is at $\tilde{x} = s_1^2/\sqrt{s_1^2 + s_2^2}$, as illustrated in Fig. 4(a). On its left and right subintervals $s(\boldsymbol{r})$ linearly depends on $\tilde{x}$, respectively. With some geometric calculations, we derive

$$P_F(\boldsymbol{r}) = \frac{1}{s(\boldsymbol{r})} = \begin{cases} \frac{s_2}{s_1} \cdot \frac{1}{\sqrt{s_1^2 + s_2^2} - \tilde{x}}, & 0 \le \tilde{x} \le \frac{s_1^2}{\sqrt{s_1^2 + s_2^2}} \\ \frac{s_1}{s_2} \cdot \frac{1}{\tilde{x}}, & \frac{s_1^2}{\sqrt{s_1^2 + s_2^2}} \le \tilde{x} \le \sqrt{s_1^2 + s_2^2} \end{cases} \tag{12}$$

$$I_2 = \int_{z=0}^{l_3} \int_{\tilde{x}=0}^{\sqrt{s_1^2+s_2^2}} P_F(\boldsymbol{r}) \mathrm{d}\tilde{x}\mathrm{d}z = l_3 \frac{s_2}{s_1} \ln \frac{s_1^2 + s_2^2}{s_2^2} + l_3 \frac{s_1}{s_2} \ln \frac{s_1^2 + s_2^2}{s_1^2}. \tag{13}$$

Its special case is $s_1 = s_2$, which results in $I_2 = 2l_3 \ln 2$.

For type-III face, the situation is more complicated. Look at its 2-D view in Fig. 5 and 3-D view in Fig. 6. The triangle face can be divided into six parts by the three altitudes. On each part, $s(\boldsymbol{r})$ is a linear function of two local variables. With the blue right-angle triangle in Fig. 6 perpendicular to the face, we can derive the values of $s(\boldsymbol{r})$ when $\boldsymbol{r}$ is at the triangle's vertex, the foot of the altitude, or the triangle's orthocenter. They are denoted by d_v, d_m, and d_c, respectively. Then, we can derive the expressions of $s(\boldsymbol{r})$ and $P_F(\boldsymbol{r})$. For example, for the bottom-left part of the triangle ("A" in Fig. 5), and supposing $s_1 = s_2 = s_3 = s$,

$$P_F(\boldsymbol{r}) = \frac{1}{\sqrt{3}s - \sqrt{6}\tilde{x}/2 - \sqrt{2}\tilde{y}/2}, 0 \le \tilde{x} \le \frac{\sqrt{2}}{2}s, 0 \le \tilde{y} \le \frac{\sqrt{3}}{3}\tilde{x}. \tag{14}$$

Finally, the integral on the type-III face is: $I_3 = 3s\ln(4/3)$.

The sampling on type-I face is trivial, which is a uniform sampling. For sampling type-II and type-III faces we can use the rejection sampling technique [9] based on the known $P_F(\boldsymbol{r})$. Then, the next random-walk position $\boldsymbol{r}_{\text{out}}$ is calculated.

B. Handling Multirectangle Floating Metals

The MIM capacitor involves floating metals in multirectangle shape (see Fig 7). Note that (10) still holds and the integral surface Γ can be

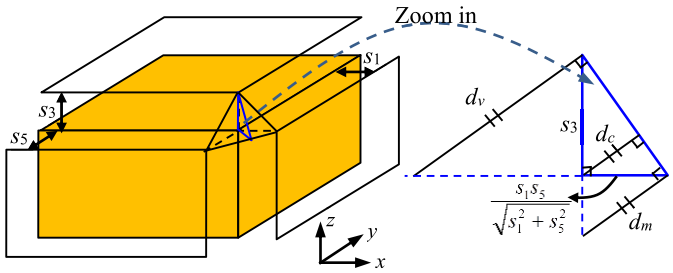

Fig. 6. Type-III face of integral surface and the related calculation of $s(\boldsymbol{r})$.

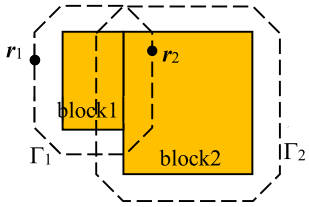

Fig. 7. Top view: multirectangle floating metal and its integral surface.

constructed similarly. To simplify the construction and the sampling process, we consider a multirectangle metal as a combination of multiple blocks (cuboids). Then, we just construct the integral surface for each block, and then make sampling on the blocks' integral surfaces and utilize the rejection sampling technique [8], [9]. Take Fig. 7 as an example. We first randomly select Γ_1 or Γ_2 according to their areas, and then randomly choose a point $\boldsymbol{r}$ on the selected block integral surface. According to $\boldsymbol{r}$'s position we decide whether to accept it or not. Points like $\boldsymbol{r}_1$ are legal points and should be accepted. On contrary, $\boldsymbol{r}_2$ is not on the integral surface of the whole metal and is thus rejected. Then, with the principle of rejection sampling and each block's $P_F(\boldsymbol{r})$ calculated, we can obtain a correct sampling point, and enable the random transitions from a multirectangle floating metal.

C. Considering Multidielectric Environment and More

With the consideration of multidielectric environment, the integrals and sampling on the integral surface of a cuboid floating metal should be modified. We first consider the situation where the dielectric interface intersects the side faces of the metal. For the relevant type-I face, $P_F(\boldsymbol{r})$ becomes a piecewise constant function, whose integral is easy to calculate. For type-II face [as shown in Fig. 8(a)], it can be regarded as the combination of two single-dielectric type-II faces. The corresponding I_2 and the sampling process can also be derived.

For the situation, where the dielectric interface is near the top/bottom face of the metal, making $\boldsymbol{r}_{\text{out}}$ on the other side of the interface [see Fig. 8(b)], the derivation from (7) to (10) does not hold. We shall use the equivalent permittivity $\varepsilon(\boldsymbol{r})$ for the region spanning from the floating metal to the sampling surface [10]. Take Fig. 8(b) as an example

$$\varepsilon(\boldsymbol{r}) = \frac{2s}{\frac{\gamma}{\varepsilon_1} + \frac{2s-\gamma}{\varepsilon_2}} = \frac{2s\varepsilon_1\varepsilon_2}{\gamma\varepsilon_2 + (2s-\gamma)\varepsilon_2}, \tag{15}$$

where γ is the distance between the interface and the floating metal. With it the approach in Section III-A becomes workable.

Calculating the electric potential of a floating metal is also important for checking the breakdown concern in the design of MIM capacitor. Suppose among the total *npath* walks there are N_k walks which first encounter No. k floating metal (denoted by F_k). And, among these N_k walks, n_k walks finally terminate at the master conductor i. Then, based on (10) and the Monte Carlo principle,

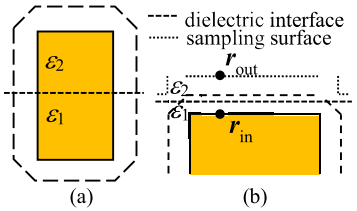

Fig. 8. Side view: cuboid floating metal and the dielectric interface. (a) Interface intersects the metal. (b) Interface is near the top/bottom face of metal.

TABLE I
RESULTS FOR THE TEST CASES WITH FLOATING DUMMY FILLS

Case	Raphael	Approach in [4]			Proposed approach		
	Cap. (aF)	Cap. (aF)	Error(%)	Time(s)	Cap. (aF)	Error(%)	Time(s)
1	2470	2477	**0.3**	6.8	2469	**-0.0**	6.8
2	753.2	746.6	**-0.9**	8.8	748.7	**-0.6**	8.6
3	741.6	735.8	**-0.8**	7.3	736.1	**-0.7**	7.5
1*	1849	1868	**1.0**	4.9	1859	**0.5**	5.0
2*	666.8	667.3	**0.1**	5.3	667.8	**0.2**	5.4
3*	570.8	565.8	**-0.9**	4.5	568.1	**-0.5**	4.6

* Single-dielectric cases obtained by setting all permittivities to 2.9.

we have: $\phi(F_k) \approx n_k/N_k$. Accordingly, its statistical error (1-σ error) can also be calculated.

IV. Numerical Results

We have implemented the approaches for handling floating metals into the program RWCap [7], [8]. An extension of [4], which incorporates the simple setting of neighborhood boundary with the technique in Section III-B, is also implemented for handling multirectangle floating metals. For all approaches, we make each face of floating metal have same distance d to the sampling surface. Raphael with dense grid discretization is used to validate the accuracy. All experiments are carried out with serial computing on a Linux server with Intel Xeon E5-2650 2.0GHz CPU. The unit of all lengths is μm.

A. Results on Cases With Floating Dummy Fills

The first three test cases are obtained from [6]. They are structures of interconnect wires including 24, 34, and 53 dummies, respectively. The size of each dummy is $1\times1\times0.6$ or $0.5\times0.5\times0.5$. The minimum spacing around a dummy is 0.6 or 0.25, accordingly. Setting 0.3% 1-σ error of the total capacitance as the termination criterion, we run the FRW-based algorithms and obtain the results listed in Table I. d is set to the minimum spacing for every case.

From Table I we see that the proposed approach has the similar runtime as the approach in [4], while the latter often shows larger error on capacitance. We have also investigated the trends of the calculated capacitance for varied d parameter. The results reveal that the both approaches are indistinguishable. The approach in [4] well handles the dummy fill with shape similar to sphere [recall the discussion on Fig. 3(b)].

B. Results on Cases of MIM Capacitor

Two kinds of MIM capacitor structures are constructed, which produces Cases 4–6. Their cross section view is like those in Fig. 1(b) and (c). Their layouts are shown in Figs. 9 and 10, with some coordinates labeled. Case 5 is obtained by a little modification on case 4 (cutting off a bottom-left corner block, in size 3×4, from the layer-n floating metal). For each case the coupling capacitance between conductors 1 and 2 is computed.

To reveal the advantage of the approach proposed in Sections III-A and III-B, we calculate the capacitance of each

TABLE II
COMPUTATIONAL RESULTS FOR THREE MULTIDIELECTRIC MIM CAPACITOR CASES

Case	Raphael				The approach in [4] or its extension						Proposed approach					
	Cap(aF)	V_1(V)	V_2(V)	V_3(V)	Cap(aF)	Error(%)	Time(s)	V_1(V)	V_2(V)	V_3(V)	Cap(aF)	Error(%)	Time(s)	V_1(V)	V_2(V)	V_3(V)
4	483.5	0.3726	0.4656	--	485.4	**0.4**	74.3	0.3806	0.4855	--	483.4	**-0.0**	76.3	0.3818	0.4787	--
5	468.1	0.367	0.443	--	460.8	**-1.6**	83.3	0.376	0.465	--	472	**0.8**	81.0	0.374	0.454	--
6	603.6	0.797	0.429	0.112	609	**0.9**	88.2	0.782	0.429	0.122	600.4	**-0.5**	88.1	0.795	0.429	0.114

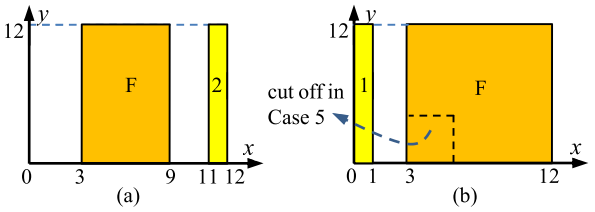

Fig. 9. 2-D layouts of an MIM structure with floating metals (cases 4 and 5). (a) Layer n-1. (b) Layer n.

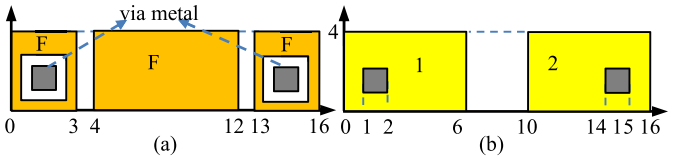

Fig. 10. 2-D layouts of another MIM structure (case 6). (a) Layer n-1. (b) Layer n.

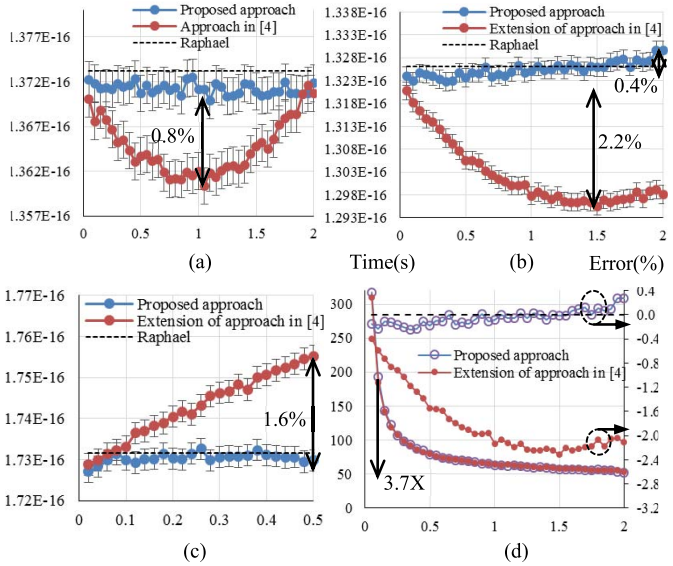

Fig. 11. (a)–(c) Capacitance value (with $\pm 3\sigma$ error bars) versus the d value for cases 4–6, respectively. (d) Runtime trends and error trends for case 5.

case with varied d value. The trends of calculated capacitance are shown in Fig. 11(a)–(c). To suppress the stochastic error, a small 0.05% 1-σ error is set as the termination criterion. Then, the shown error is mainly the systematic error with respect to Raphael's result. From these figures we see that with the approach in [4] and its extension the systematic error can be very large, while the proposed approach keeps reasonable accuracy even for the largest d (the minimum distance between a floating metal and other conductors). For case 5, larger d value causes the systematic error of approach in [4] increasing from less than 0.5% to larger than 2.2%, while that of the proposed approach keeps within 0.4% (5× less). This is more clearly shown in Fig. 11(d). If using a naïve implementation of the approach of [4], which has a cuboid sampling surface for each floating metal, we see even larger systematic error (up to −40%) for some d.

We draw Fig. 11(d) to reflect how d affects the runtime of the approaches and their errors to Raphael. It reveals that the proposed approach and that in [4] have almost the same runtime-vs-d trend, but different errors. With same 0.5% systematic error, the proposed approach is over 3.7× faster than the extension of existing approach (52 s at $d = 2$ versus 193 s at $d = 0.1$).

Assuming an environment with three dielectric layers with permittivities 1.9, 2.9, and 3.9, we simulate the multidielectric cases with 0.3% 1-σ error for termination and list the results in Table II. From it we confirm again that the proposed approach is more accurate than the extension approach of [4] on both capacitance and the voltage of floating metal (e.g., see the results on V_3), while the latter's results often violate the 3σ error range due to the larger systematic error.

V. CONCLUSION

For the structure including general-shape floating metals, we propose a reliable and accurate FRW-based approach to calculate capacitances. It allows larger hops from the floating metal while keeping small systematic error, and thus reduces the overall runtime. With the rejection sampling, the approach is extended to handle multirectangle floating metals in MIM capacitor structures. This makes the proposed approach a practical tool for the design of high-density MIM capacitor.

REFERENCES

[1] M. Bohr, "Silicon technology leadership for the mobility era," presented at the Intel Developer Forum (IDF), San Francisco, CA, USA, 2012.
[2] J. S. Dunn, Z.-X. He, and A. K. Stamper, "Method of manufacturing complimentary metal-insulator-metal (MIM) capacitors," U.S. Patent 8 857 022 B2, 2014.
[3] K. Fischer *et al.*, "Low-k interconnect stack with multi-layer air gap and tri-metal-insulator-metal capacitors for 14nm high volume manufacturing," in *Proc. IEEE IITC/MAM*, Grenoble, France, 2015, pp. 5–8.
[4] S. Batterywala, R. Ananthakrishna, Y. Luo, and A. Gyure, "A statistical method for fast and accurate capacitance extraction in the presence of floating dummy fills," in *Proc. 19th Int. Conf. VLSI Design*, Jan. 2006, pp. 129–134.
[5] D. Xiang, K. Chakrabarty, and H. Fujiwara, "Multicast-based testing and thermal-aware test scheduling for 3D ICs with a stacked network-on-chip," *IEEE Trans. Comput.*, vol. 65, no. 9, pp. 2767–2779, Sep. 2016.
[6] W. Yu, M. Zhang, and Z. Wang, "Efficient 3-D extraction of interconnect capacitance considering floating metal fills with boundary element method," *IEEE Trans. Comput.-Aided Design Integr. Circuits Syst.*, vol. 25, no. 1, pp. 12–18, Jan. 2006.
[7] W. Yu, H. Zhuang, C. Zhang, G. Hu, and Z. Liu, "RWCap: A floating random walk solver for 3-D capacitance extraction of very-large-scale integration interconnects," *IEEE Trans. Comput.-Aided Design Integr. Circuits Syst.*, vol. 32, no. 3, pp. 353–366, Mar. 2013.
[8] C. Zhang and W. Yu, "Efficient techniques for the capacitance extraction of chip-scale VLSI interconnects using floating random walk algorithm," in *Proc. ASP-DAC*, Jan. 2014, pp. 756–741.
[9] W. H. Press, S. A. Teukolsky, W. T. Vetterling, and B. P. Flannery, *Numerical Recipes in C*, 2nd ed. Cambridge, U.K.: Cambridge Univ. Press, 1992.
[10] Z. Ren and C. Lage, "3-D capacitance extraction of IC interconnects using field solvers and homogenization technique," *IEEE Trans. Magn.*, vol. 40, no. 2, pp. 703–706, Mar. 2004.